Available online at www.sciencedirect.com
ScienceDirect
Journal of Catalysis 245 (2007) 237–248
JOURNAL OF CATALYSIS
www.elsevier.com/locate/jcat

Tailoring Raney-catalysts for the selective hydrogenation of butyronitrile to *n*-butylamine

Adam Chojecki, Maritza Veprek-Heijman, Thomas E. Müller *, Peter Schärringer, Stan Veprek, Johannes A. Lercher

Technische Universität München, Department Chemie, Lichtenbergstraße 4, 85747 Garching, Germany

Received 17 July 2006; revised 5 October 2006; accepted 6 October 2006

Abstract

The influence of LiOH promotion on Co-based Raney-catalysts for the selective hydrogenation of butyronitrile to *n*-butylamine was explored. Doping with LiOH led to an increase in the fraction of metallic surface area and reduced concentration of Lewis acid sites resulting from alumina particles decorating the metal surface. Two factors were found to be crucial to achieving high selectivity to primary amines. These factors include a low adsorption constant of *n*-butylamine relative to butyronitrile (because adsorbed butylamine is necessary for byproduct formation) and a low concentration of Lewis acid sites catalyzing condensation reactions.

Keywords: Nitrile; Amine; Hydrogenation; Selectivity; Raney-catalyst; Cobalt; Nickel; Lithium hydroxide; Surface modification; Lewis acid site; Adsorption constant; Polarization effect; Condensation reaction

1. Introduction

The reduction of nitriles to primary amines is a large-scale commercial process route [1]. One of the most important applications is the conversion of 1,4-dicyanobutane to 1,6-diaminohexane, which is used in the production of nylon-6,6 [2,3]. It is known that the hydrogenation of C≡N groups proceeds stepwise through reactive intermediates [4,5]. Consequently, condensation reactions may occur and mixtures of ammonia and primary, secondary, and tertiary amines are generally obtained. The factors that influence the product distribution are manifold and originate from catalyst composition (e.g., choice of metal and support, presence of promoters) and reaction conditions [6]. High selectivities to primary amines were reported for Co, Ni, and Ru catalysts [7]. In contrast, nitriles can be reduced to secondary and tertiary amines using Rh, Pd, and Pt catalysts [8]. In the industrial process, a high selectivity to primary amines is achieved by working at high hydrogen pressures (up to 600 bar) and with ammonia as solvent [9]. Skeletal metal catalysts based on Ni and Co provide the lowest cost per unit mass of active catalyst and are widely used [10]. Their selectivity can be enhanced by modification with small amounts of alkali metal hydroxides [11–13]. The reduction of nitriles with Raney-Ni has been studied repeatedly [14–16], whereas fewer reports have been published on Raney-Co [17–20]. For Raney-Ni, the effect of bases on selectivity also has been investigated [21,22].

The rational development of next generation catalysts with high specifity to primary amines requires deeper insights into the processes that govern selectivity. Consequently, the present study was aimed at establishing for the first time correlations between the surface properties of unmodified and LiOH-doped Raney-Co catalyst, the sorption characteristics for hydrogen as well as nitrile and amine, and the catalytic activity in the reduction of nitriles. The hydrogenation of butyronitrile to *n*-butylamine was explored as a model reaction for the reduction of nitriles over Raney catalysts (Scheme 1). Several techniques for the characterization of Raney catalysts were used, focusing on surface properties. Special emphasis was placed on understanding the beneficial effect of LiOH modification on the intrinsic activity and selectivity of Raney-Co. As ref-

* Corresponding author.
E-mail address: Thomas.Mueller@ch.tum.de (T.E. Müller).

0021-9517/$ – see front matter
doi:10.1016/j.jcat.2006.10.012

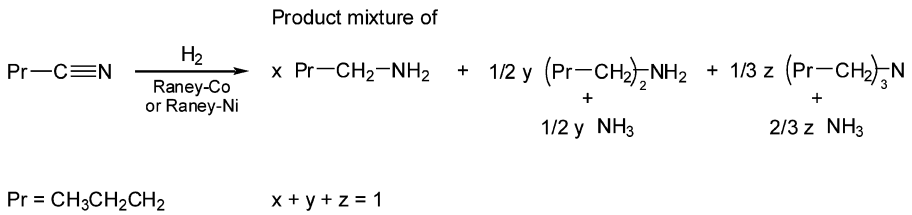

Scheme 1.

erence materials, commercial catalysts with low selectivity but relatively high activity (Raney-Ni), high selectivity and low activity (Raney-Co), and both high selectivity and high activity (Ni–Cr-promoted Raney-Co) were chosen. For those materials, the characterization was aimed at establishing boundary conditions for designing catalysts for the selective hydrogenation of nitriles to primary amines.

2. Experimental

2.1. Catalyst preparation and materials

The catalysts Raney-Ni (#2800, lot #7716, mean grain diameter 45.6 μm), Raney-Co (#2700, lot #7865, mean grain diameter 30.1 μm), and Ni–Cr-promoted Raney-Co (#2724, lot #7733, mean grain diameter 28.5 μm) were obtained as an aqueous suspension from W.R. Grace & Co, GRACE Davison Chemical Division (see Table 1 for chemical composition). Catalysts used for characterization and hydrogenation experiments underwent the following pretreatment. The catalysts were washed with deionized water until pH 7 was reached, taking care that the catalyst was sufficiently covered with liquid to prevent contact with atmospheric oxygen. After drying in a flow of argon (4 h at 328 K, followed by 1 h at 378 K), the catalysts were handled and stored under inert atmosphere throughout all other preparation and characterization steps. For doping with LiOH, a thoroughly washed 143-g sample of Raney-Co was suspended in an aqueous solution of LiOH (3.25 g in 100 cm^3 of deionized water). The water was removed in partial vacuum (<4 mbar), and the sample was dried (10 h at 323 K). The concentration of Li^+ was 0.5 wt% Li as determined by atomic absorption spectrometry (UNICAM 939 AA-Spectrometer).

All other chemicals used in this study were obtained from commercial suppliers and used as received (butyronitrile, ⩾99% GC-assay, Fluka; mono-, di-, and tri-*n*-butylamine, >99% GC-assay, Aldrich; *n*-octane and *n*-undecane, ⩾99 GC-assay, Aldrich; and H_2, Ar, NH_3, 99.999, 99.999, and 99.98 vol%, respectively). All solvents and reactants were degassed in partial vacuum.

Table 1
Chemical composition of the catalysts used in this study (data of catalyst manufacturer)

Catalyst	Element			
	Co [wt%]	Ni [wt%]	Cr [wt%]	Al [wt%]
Raney-Ni	<0.5	92.8	–	6.77
Raney-Co	97.5	<0.5	<0.5	1.85
Ni–Cr-promoted Raney-Co	91.3	2.8	2.2	3.50

2.2. Catalysis

The hydrogenation of butyronitrile was carried out in a high-pressure 160 cm^3 semibatch reactor at constant hydrogen pressure. Oxygen was removed from the autoclave through several cycles of pressurizing and depressurizing with argon. The autoclave was then charged under a flow of argon with 50 cm^3 of reaction mixture, composed of butyronitrile (2.18 cm^3, 0.025 mol, corresponding to 0.5 mol dm^{-3}), octane (47.6 cm^3), and catalyst (0.2 g), with *n*-undecane (0.2 g) added as an internal standard for GC chromatography. The mixture was stirred at 1500 rpm and equilibrated at the reaction temperature (373 K) for 45–60 min. The reaction was started by rapidly pressurizing the autoclave with hydrogen to 15, 30, or 45 bar. During the experiment, samples of the liquid phase were taken for off-line GC analysis with an HP 5890 gas chromatograph equipped with a cross-linked 5% diphenyl–95% dimethylpolysiloxane column (Rtx-5 Amine, 30 m, Restek GmbH). The reaction rate was calculated from the decrease in butyronitrile concentration in the linear range between 20 and 80% conversion. A test on mass transfer limitations showed that the reaction rate did not depend on the stirring speed in the range of 1000–1850 rpm.

2.3. Catalyst characterization

N_2-physisorption and H_2-chemisorption measurements were carried out on a Sorptomatic 1990 instrument (ThermoFinnigan). For N_2-physisorption, the catalyst samples (0.4–1.0 g) were outgassed for 1 h under high vacuum at a prespecified temperature (298–633 K). The measurements were carried out at 77 K using N_2 as a probe molecule. BET area and pore volume were calculated from the isotherm. The micropore volume was calculated from a Horvath–Kawazoe plot in the pressure range of $p/p^\circ = 0$–0.2. For hydrogen chemisorption, the catalysts were outgassed for 1 h at 383 K. Isotherms were recorded at 298 K, with equilibration for 2–180 min for each pressure step. Equilibration was continued until the pressure deviation was <0.27 mbar within of a 2-min period. Isotherms were measured twice on the same sample. Between the two measurements, the sample was evacuated to 10^{-3} mbar for 1 h. The second isotherm (physisorbed H_2) was subtracted from the first isotherm (chemisorbed and physisorbed H_2). To determine the amount of chemisorbed hydrogen, the linear part of the isotherm at $p > 3$ Pa was extrapolated to zero. The fraction

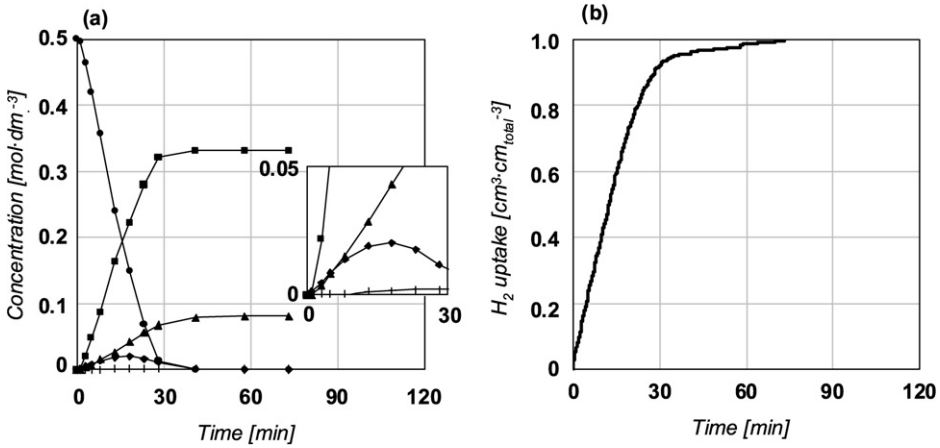

Fig. 1. (a) Concentration profile for the hydrogenation of butyronitrile over Raney-Ni at 373 K, $p = 30$ bar, c_0 (butyronitrile) = 0.50 mol dm^{-3} (●, butyronitrile; ■, *n*-butylamine; ▲, di-*n*-butylamine; ◆, *N*-butylidene-butylamine; +, tri-*n*-butylamine). (b) Integral hydrogen uptake.

of accessible metal atoms was calculated assuming that one hydrogen atom was adsorbed per nickel or cobalt atom.

Temperature-programmed desorption (TPD) measurements were carried out in a custom-built vacuum setup. The catalyst (50 mg) was outgassed for 8 h at 378 K. The temperature was then raised at a rate of 10 K min^{-1} to 973 K, and the desorbing molecules were analyzed by mass spectrometry. The masses $m/z^+ = 2$ and 18 were used for monitoring desorption of hydrogen and water, respectively. To determine the desorption maxima, the MS traces were fitted with Gaussian curves using Grams/AI (Thermo Galactic, version 7.02). For TPD of ammonia, the sample (100 mg) was heated in high vacuum at 5 K min^{-1} to 473 K, outgassed for 5 min, and cooled to 423 K. Then the sample was equilibrated for 1 h with ammonia ($p_{NH_3} = 1 \pm 0.3$ mbar), outgassed for 3 h, and finally heated at a rate of 10 K min^{-1}. Ammonia desorption was followed by MS using $m/z^+ = 15$.

For X-ray photoelectron spectroscopy (XPS) measurements, care was taken to avoid contact of the catalyst samples with atmospheric oxygen. In a glove box, the dried catalyst was placed on adhesive conducting tape. The sample was transferred under Argon to a Leybold LH 10 surface analysis system and analyzed without further pretreatment. For each sample, a survey spectrum was collected. The detailed spectra were excited with AlK_α (1486.6 eV, 0.83 nm) and recorded in ΔE = constant mode. Selected spectral regions were repetitively scanned, and the signals were averaged to improve the signal-to-noise ratio. To compensate for charge effects, the C 1s signal at 285 eV was used as a reference [23], and the binding energy scale was corrected. Data were fitted (solid lines in Fig. 7) to account for the different species on the catalyst surface. Spectral resolution and error in the peak position was approximately 0.5 eV.

The adsorption constants were calculated from breakthrough curves, which were obtained in a custom-built setup. A chromatographic column was packed under argon with the dried catalyst (2.5 g). The void spaces below and above the catalyst were filled with glass beads. Using a bypass, all lines were flushed with argon before the experiments. The column was equilibrated at room temperature with thoroughly degassed *n*-pentane. A solution of the adsorbate (*n*-butylamine or butyronitrile) and internal standard (octane) in *n*-pentane (both 12.5 mmol dm^{-3}) was passed over the catalyst at constant rate (2.2–2.3 cm^3 min^{-1}). The effluent was sampled every 0.2 min until steady state was obtained at the exit of the column. The composition of the eluent was evaluated by gas chromatography. The concentration of the adsorbate in the feed was then increased stepwise to 12.5, 25, 50, 75, and 100 mmol dm^{-3}. For competitive sorption, an equimolar solution of *n*-butylamine and butyronitrile (50 mmol dm^{-3}) was passed over the catalyst.

3. Results

3.1. Catalytic activity in the reduction of butyronitrile and selectivity to n-butylamine

Activity and selectivity of four different Raney catalysts (Raney-Ni, Raney-Co, Ni–Cr-promoted Raney-Co, and LiOH-modified Raney-Co) were tested for the hydrogenation of butyronitrile. A typical concentration profile for Raney-Ni is shown in Fig. 1a. After a short induction time (2 min), the hydrogenation of butyronitrile proceeded at a rate of 0.97×10^{-4} mol$_{\text{butyronitrile}}$ ($g_{\text{cat.}}$ s)$^{-1}$. The butyronitrile concentration decreased almost linearly with time. In parallel, the integral hydrogen consumption increased linearly (Fig. 1b). Only at high conversions (>80%), the rate of reaction decreased. The main product was *n*-butylamine, which was formed with 66% selectivity. Di-*n*-butylamine and traces of tri-*n*-butylamine were formed as byproducts; *N*-butylidene-butylamine was observed as a reaction intermediate (maximum concentration, 20×10^{-3} mol dm^{-3}). Its concentration began to decrease as soon as >70% of butyronitrile had been converted. At the end of the experiment, no *N*-butylidene-butylamine was found. The concentrations of *n*-butylamine and *N*-butylidene-butylamine began to increase immediately after the start of the reaction, indicating that both are primary reaction products. In contrast, di-*n*-butylamine and tri-*n*-butylamine were formed with a time delay, suggesting that they are secondary reaction products.

A typical concentration profile for the hydrogenation of butyronitrile over Raney-Co is related to the integral hydrogen

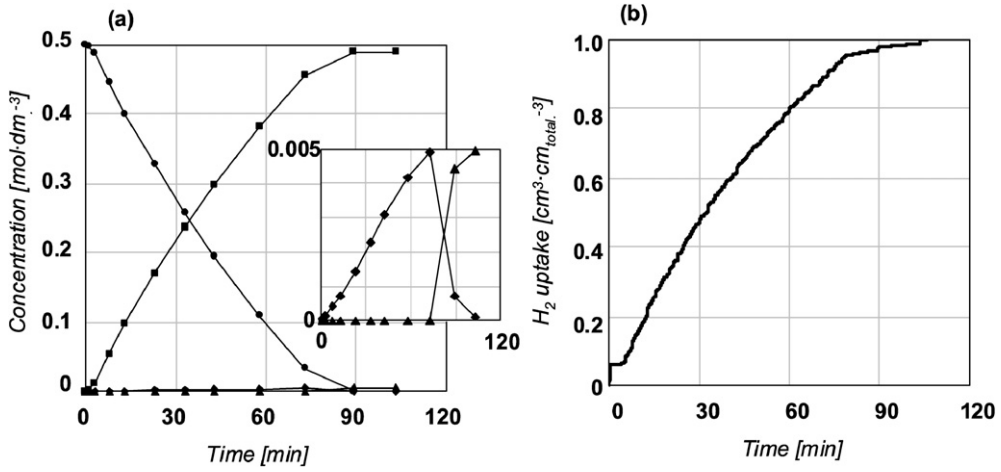

Fig. 2. (a) Concentration profile during the hydrogenation of butyronitrile over Raney-Co at 373 K, $p = 30$ bar, c_0 (butyronitrile) = 0.50 mol dm^{-3} (●, butyronitrile; ■, *n*-butylamine; ▲, di-*n*-butylamine; ◆, *N*-butylidene-butylamine; +, tri-*n*-butylamine). (b) Hydrogen uptake normalized to the total H_2-uptake.

Table 2
Activity and selectivity of Raney catalysts in the hydrogenation of butyronitrile

Catalyst	Rate normalized to catalyst weight [$mol_{butyronitrile}$ ($g_{cat.}$ s)$^{-1}$]	Rate normalized to accessible metal atoms [$mol_{butyronitrile}$ ($mol_{surface\ atoms}$ s)$^{-1}$]	Selectivity [%]
Raney-Ni	0.97×10^{-4}	0.14	66.0
Raney-Co	0.33×10^{-4}	0.08	98.0
Ni–Cr-promoted Raney-Co	2.47×10^{-4}	0.31	99.0
LiOH-modified Raney-Co	0.39×10^{-4}	0.22	99.5

consumption in Fig. 2. After a short induction period (<3 min), the hydrogenation commenced at a rate of 3.25×10^{-5} $mol_{butyronitrile}$ ($g_{cat.}$ s)$^{-1}$ and was completed after 90 min. The selectivity to *n*-butylamine was high (98.0%). *n*-Butylamine and *N*-butylidene-butylamine were detected immediately after the start of the reaction and appeared to be primary reaction products. The formation of di-*n*-butylamine was only observed after >90% of the butyronitrile had been hydrogenated. It is particularly noteworthy that the final concentration of di-*n*-butylamine was equal to the maximum concentration of *N*-butylidene-butylamine. This strongly suggests that di-*n*-butylamine is a sequential product of the hydrogenation of *N*-butylidene-butylamine. Tri-*n*-butylamine was not found.

Over Ni–Cr-promoted Raney-Co and LiOH-modified Raney-Co, the reaction proceeded in a similar way as with Raney-Co but with improved activity [2.47×10^{-4} and 0.39×10^{-4} $mol_{butyronitrile}$ ($g_{cat.}$ s)$^{-1}$, respectively] and selectivity to *n*-butylamine (99.0 and 99.5%, respectively). In addition, the maximum concentrations of *N*-butylidene-butylamine (2.0×10^{-3} and 1.0×10^{-3} mol dm^{-3}, respectively) were lower than with the parent Raney-Co (4.9×10^{-3} mol dm^{-3}). As with Raney-Co, the final concentration of di-*n*-butylamine was equal to the maximum transient concentration of *N*-butylidene-butylamine. Note that *N*-butylidene-butylamine was hydrogenated to di-*n*-butylamine only at high butyronitrile conversions.

The intrinsic activity (normalized to the number of accessible metal atoms) is compared with the weight normalized catalytic activity in Table 2. The sequence in the activity of the four catalysts depends on the definition of the activity. This indicates that the differences in activity are not a mere consequence of the number of metal surface atoms, but rather represent intrinsic differences in the nature of the catalytically active sites. Consequently, a detailed characterization of the catalysts seemed to be necessary.

3.2. Specific surface area and fraction of accessible metal atoms

The BET surface area of Raney-Ni and Raney-Co varied with the temperature applied for outgassing the samples before the measurements (Table 3). For Raney-Ni, the largest BET area was measured after activation at 383 K (58 $m^2\ g_{cat.}{}^{-1}$), whereas the maximum for Raney-Co was observed after outgassing at 483 K (25 $m^2\ g_{cat.}{}^{-1}$). Lower activation temperatures were probably insufficient to completely remove the adsorbates from the catalyst pores, whereas higher temperatures led to particle sintering. The higher activation temperature required for Raney-Co indicates that adsorbates, such as water and hydrogen, were bound more strongly than on Raney-Ni. However, the differences caused by changing the activation temperature were small compared with the variations among the four catalysts. The BET surface area was higher for Raney-Ni (58 $m^2\ g_{cat.}{}^{-1}$) than for Raney-Co (19 $m^2\ g_{cat.}{}^{-1}$). The presence of promoters, as in Ni–Cr-promoted Raney-Co, stabilized a high BET surface area (67 $m^2\ g_{cat.}{}^{-1}$). In contrast, the LiOH-modified Raney-Co had a lower surface area (15 $m^2\ g_{cat.}{}^{-1}$). Note that after LiOH modification of Raney-Co, the pore volume (0.094 $cm^3\ g_{cat.}{}^{-1}$) did not change (within the limits of experimental error); however, the volume of the pores with diameter

⩽1.0 nm decreased from 0.008 to 0.006 $cm^3\ g_{cat.}{}^{-1}$. This suggests that LiOH resided mostly in the small pores, which contribute little to the void volume but significantly to the surface area.

The fraction of surface metal atoms was determined by hydrogen chemisorption (Fig. 3, Table 4). For the four catalysts, the same trend was observed as that based on the BET surface area; however, the metal surface area was roughly two times lower than the specific surface area. This demonstrates that only a part of the surface was accessible nickel or cobalt. Most likely, aluminum not removed during preparation [21,24,25], Al_2O_3, and other oxides led to a higher specific surface area and covered part of the catalytically active metal surface.

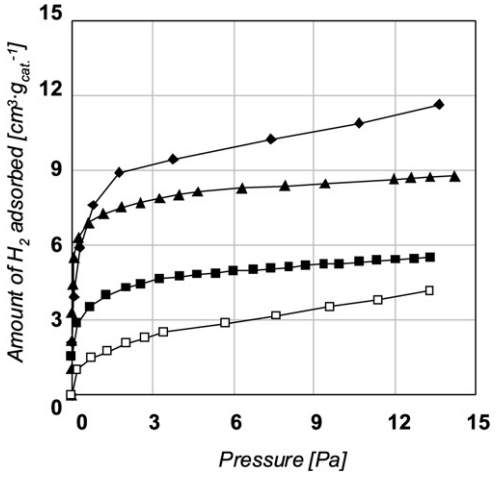

Fig. 3. Hydrogen adsorption isotherms recorded at 298 K (◆, Ni–Cr-promoted Raney-Co; ▲, Raney-Ni; ■, Raney-Co; □, LiOH-modified Raney-Co).

Table 3
BET surface area measured after outgassing the catalyst samples for 1 h at the temperature stated

$T_{activation}$ [K]	Raney-Ni [$m^2\ g_{cat.}{}^{-1}$]	Raney-Co [$m^2\ g_{cat.}{}^{-1}$]	Ni–Cr-promoted Raney-Co [$m^2\ g_{cat.}{}^{-1}$]	LiOH-modified Raney-Co [$m^2\ g_{cat.}{}^{-1}$]
298	55.4	19.2	67.5	14.8
383	57.7	19.3	66.8	14.8
483	52.2	24.6	61.7	–
533	–	24.1	–	–
583	47.9	23.7	–	–
633	45.7	19.5	–	–

3.3. Residual water and hydrogen on the catalyst surface

The concentration of residual molecules remaining on the catalyst surface after outgassing was determined by TPD (Figs. 4 and 5 [26]). Raney-Ni exhibited a relatively narrow temperature range for desorption of water and hydrogen (400–530 K). The narrow distribution of desorption states may be related to a uniform surface structure with a low concentration of defects. In this respect, Martin et al. demonstrated, by measuring the saturation magnetization of Raney-Ni in an electromagnetic field, that the hydrogen that evolves during TPD cannot be the result of a reaction between water and metallic aluminum [27]. Thus, hydrogen evolution can originate only from hydrogen that remained adsorbed on the material after the preparation procedure. Note that this process involves dissolution of aluminum in an aqueous base under the evolution of hydrogen.

For the parent and Ni–Cr-promoted Raney-Co, the TPD traces of both residual water and hydrogen showed a broad temperature range for desorption (400–730 K). For hydrogen, the rather difficult deconvolution of the data allows only a quali-

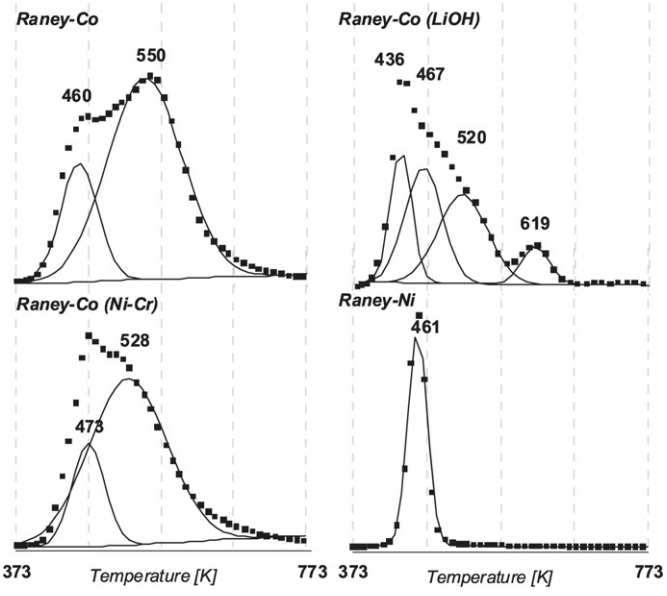

Fig. 4. TPD traces of residual water (■) for the Raney-catalysts studied and contribution of single sites (solid lines).

Table 4
Number of Ni or Co surface atoms and metal surface area as determined by H_2-chemisorption at 298 K. For comparison, the results from N_2-physisorption are included

Catalyst	Accessible metal atoms [$mmol\ g_{cat.}{}^{-1}$]	Dispersion [%]	Metal surface area* [$m^2\ g_{cat.}{}^{-1}$]	BET surface area [$m^2\ g_{cat.}{}^{-1}$]	Pore volume [$cm^3\ g_{cat.}{}^{-1}$]
Raney-Ni	0.69	4.06	27.0	55.4	–
Raney-Co	0.40	2.35	15.7	19.2	0.094
Ni–Cr-promoted Raney-Co	0.80	4.72	31.3	67.5	–
LiOH-modified Raney-Co	0.18	1.06	7.1	14.8	0.095

* Calculated based on a stoichiometry of 1 H atom per metal atom and a transversal section of 6.5 $Å^2$ for Ni and Co.

tative discussion of the data. Note that metal sintering occurs at higher temperatures but is a relatively slow process. Because the BET area at 633 K was decreased by only about 20% relative to the maximum BET area (Raney-Ni and Raney-Co; see Table 4), we assume that the TPD measurements reflect the true state of the catalyst. In general, the desorption maxima for water and hydrogen occurred at roughly the same temperature, but the low-temperature peaks for water were much more pronounced than those for hydrogen.

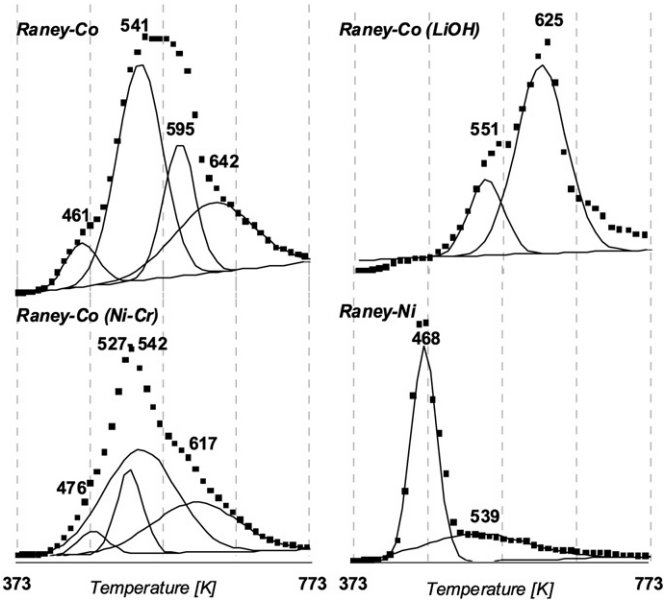

Fig. 5. TPD traces of residual hydrogen (■) for the Raney-catalysts used in this study and contribution of single sites (solid lines).

For LiOH-modified Raney-Co, analysis of the TPD data again did not exhibit a satisfying deconvolution. However, the highest rate of water desorption occurred at 436 K and decreased slowly at higher temperatures. In contrast, for the parent Raney-Co, the first desorption maximum occurred at 460 K. In this respect, it is known [28] that lithium hydroxide reacts readily with aluminum hydroxide to $LiAl_2(OH)_7 \times 2H_2O$ [29], which dehydrates at low temperatures ($\leqslant$473 K). Thus, the desorption maximum at 436 K is probably related to reaction of lithium hydroxide. A second low-intensity desorption feature at 619 K can be similarly explained by dehydration of LiOH occurring in vacuum at 623 K. The desorption peak at 619 K correlates well with a maximum hydrogen desorption at 625 K. The desorption trace of hydrogen showed two major desorption peaks at 551 and 625 K. The first hydrogen desorption maximum at 551 K is probably due to desorption of residual hydrogen from the metal surface, as for the other two Raney-Co catalysts. The second, more intense peak at 625 K is probably the result of a secondary reaction between aluminum and LiOH,

$$2\mathrm{LiOH} \longrightarrow \mathrm{Li_2O} + \mathrm{H_2}, \tag{1}$$

$$2\mathrm{Al} + \mathrm{LiOH} + 6\mathrm{H_2O} \longrightarrow \mathrm{LiAl_2(OH)_7} + 3\mathrm{H_2}, \tag{2}$$

$$2\mathrm{Al} + 13\mathrm{LiOH} \longrightarrow \mathrm{LiAl_2(OH)_7} + 6\mathrm{Li_2O} + 3\mathrm{H_2}. \tag{3}$$

3.3.1. TPD of ammonia

The acid–base properties of Raney-Ni and Raney-Co were explored through TPD of ammonia. Note that acid sites catalyze side reactions during the hydrogenation of nitriles [30]. The desorption traces of ammonia were generally broad and showed two pronounced maxima (Fig. 6). It is particularly noteworthy that for Raney-Ni, maximum H_2 desorption was asso-

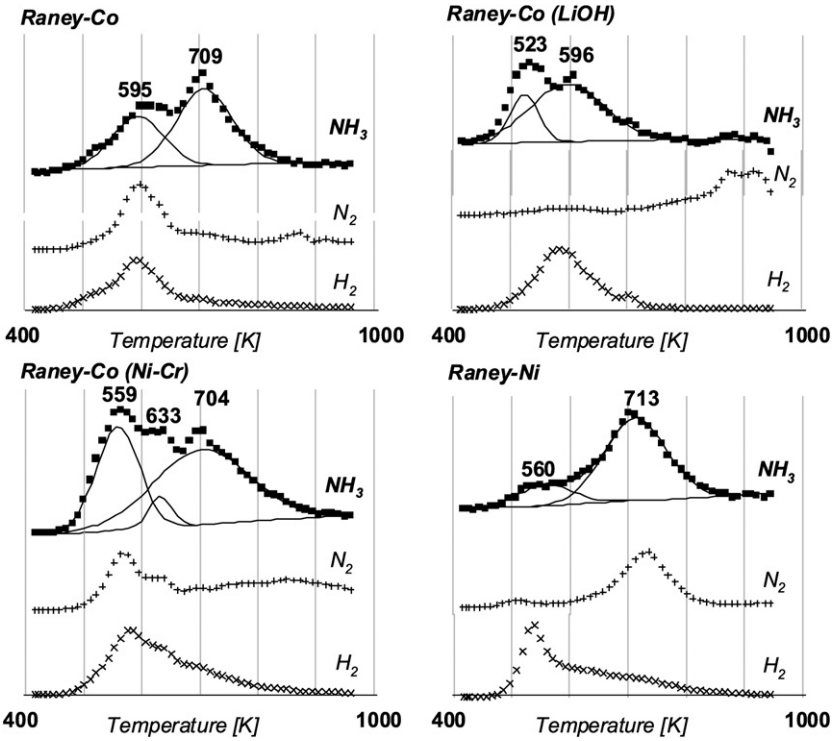

Fig. 6. TPD traces of NH_3 (■), N_2 (+) and H_2 (×) for Raney-catalysts after adsorption of NH_3 at 423 K.

ciated with the low-temperature desorption peak of ammonia at 560 K, whereas maximum N_2 desorption was related to the high-temperature peak in NH_3 desorption at 713 K. For Raney-Co, maxima in N_2 and H_2 desorption occurred in parallel with the first desorption peak of NH_3 (595 K), whereas a second maximum at 709 K was observed only for NH_3 desorption. For Ni–Cr-promoted Raney-Co, the desorption maxima were at 559 and 704 K. An additional contribution with very low intensity was detected at 633 K.

The significant differences between cobalt and nickel can be explained by considering the relative stability of cobalt and nickel nitrides [31,32]. Baiker et al. found that reaction of ammonia with nickel at temperatures above 395 K led to the formation of nickel nitride Ni_3N and molecular hydrogen [33]. Nickel nitride is stable up to 683 K but decomposes to metallic nickel and nitrogen at higher temperatures. When ammonia is adsorbed at 423 K, it partially dissociates on the Ni surface to surface hydrogen atoms and nitrenes [34]. The latter species react with nickel to form nickel nitride. As the catalyst is heated, surface-bound hydrogen and ammonia desorb first. At higher temperatures, Ni_3N decomposes, resulting in the maximum rate of nitrogen evolution at 713 K. Part of the nitrogen reacts with residual H_2 and leads to a second maximum in NH_3 desorption.

In contrast, Co_3N is less stable and decomposes when heated to 549 K [32]. Consequently, cobalt nitride is hardly formed during the adsorption of ammonia. On heating, dissociated surface species recombine to either ammonia or molecular hydrogen and nitrogen. Thus, the second maximum observed for Raney-Co at 709 K cannot be associated with metallic cobalt but instead is attributed to ammonia molecularly bound to Al^{3+} Lewis acid sites [22]. Because of the high stability, the Lewis adduct $H_3N{:}\rightarrow Al^{3+}$ decomposes only at high temperatures [35].

Compared with the parent Raney-Co, the first maximum in the ammonia trace for Ni–Cr-promoted Raney-Co was shifted to lower temperatures (559 K), indicating weaker binding of ammonia. It was associated with nitrogen and hydrogen desorption.

For the LiOH-modified Raney-Co, the NH_3 desorption trace showed a maximum at 523 K with a broad shoulder centered at 596 K. Similar to the parent Raney-Co, the peak at 596 K is tentatively attributed to NH_3 desorption from metallic cobalt. This assignment is supported by the parallel H_2 desorption. It is noteworthy that hardly any nitrogen desorbed from the sample, and we speculate that surface bound nitrenes reacted with LiOH. The low-temperature peak in the NH_3 desorption trace at 523 K is most likely molecular ammonia, which is weakly coordinated to LiOH clusters. The high-temperature peak at 709 K (Raney-Co) associated with Lewis acid sites of alumina was not observed, strongly suggesting that LiOH blocks these sites.

3.4. Characterization by XPS

The nature of different phases at the catalyst surface was evaluated by XPS (see Fig. 7). Note that the inelastic mean free path (IMPF) of the electrons for Ni and Co was ∼1.25 and

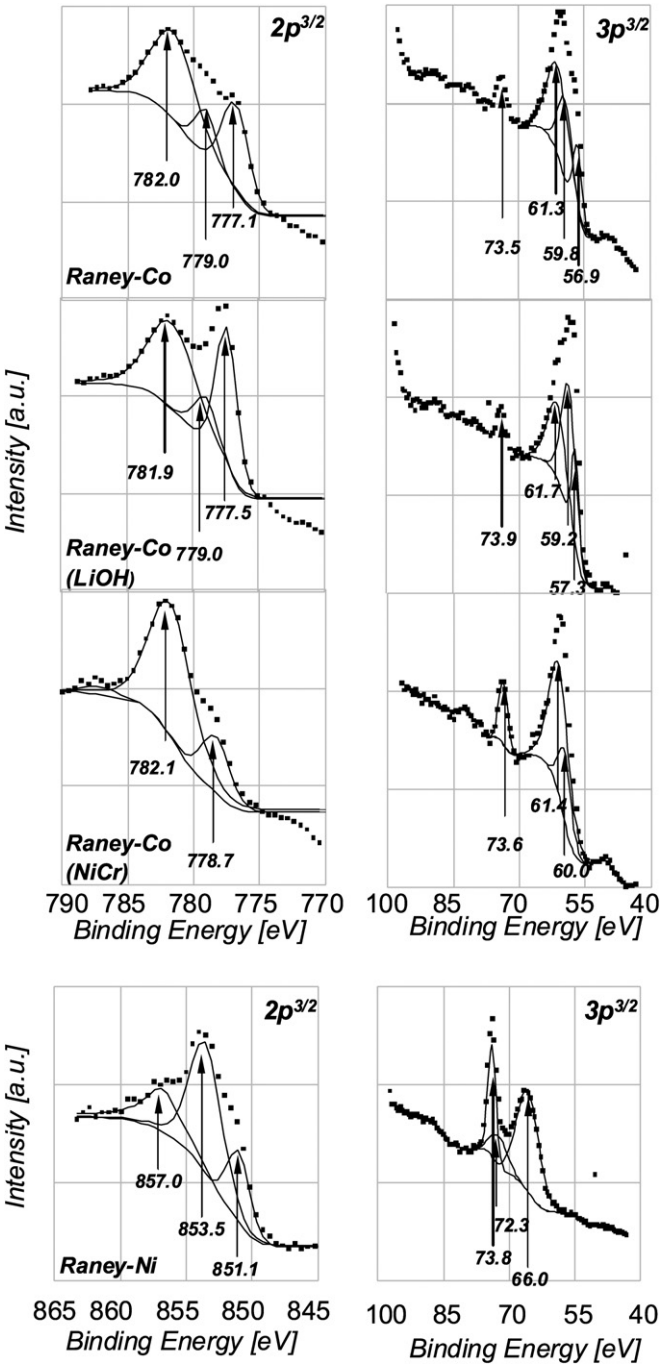

Fig. 7. XPS spectra for Raney-catalysts and contribution of single states.

1.2 nm, respectively; thus, the surface was probed to roughly this depth. Peaks that were not sufficiently separated in deconvolution are shown in the diagrams but not considered further in this discussion.

For Raney-Ni, peaks at 857.0, 853.5, and 851.1 eV were observed in the Ni $2p^{3/2}$ region. The peaks at 857.0 and 853.5 eV correspond to Ni^{2+} cations, probably $NiAl_2O_4$ (857.1 eV [36]) and NiO (853.5 eV [36]), respectively. In the literature, Ni_2O_3 [37], $Ni(OH)_2$, and $NiAl_2O_4$ [21] have also been reported at the surface of Raney-Ni catalysts; however, the peak at 853.5 eV could also be attributed to Al_3Ni alloy (853.6 eV [38]). Metal-

lic nickel (Ni^0) was observed at 851.1 eV, lower than reported previously (852.1 eV [36]).

The XPS spectra of cobalt samples exhibited two maxima at 782.0 and ∼779.0 eV in the Co $2p^{3/2}$ region. The peak at 779.0 was almost completely superposed by other peaks, and deconvolution might not afford the exact peak position. The spectra of Raney-Co and LiOH-modified Raney-Co showed an additional peak between 777.1 and 777.5 eV. The two peaks could not be clearly distinguished in the spectrum of Ni–Cr-promoted Raney-Co. Note that after LiOH treatment of Raney-Co, the intensity of the peak at 777.5 eV increased relative to the other peaks in the spectrum. The highest binding energy at 782.0 eV is probably related to oxidized cobalt in a strongly ionic ligand field. Co/Al mixed oxide is speculated to cause this peak. The photoelectron contribution at 777.1 eV shows that metallic cobalt Co^0 was present at the outermost surface [36]. The relative contribution of metallic cobalt increased significantly after LiOH modification of the surface. In this respect, it is known that Al_2O_3 can be removed from the surface of Raney-Ni by treatment with bases, such as NaOH [21].

The $3p^{3/2}$ region was also analyzed; the IMPF was ∼0.37–0.40 for nickel and 0.36–0.40 nm for cobalt. Note that, compared with the Co and Ni $2p^{3/2}$ region, the XPS spectrum in the $3p^{3/2}$ region bears more information about the catalyst composition on the surface.

The spectrum of Raney-Ni showed a peak at 73.8 eV, an intense peak at 66.0 eV, and a small contribution between those two peaks. Spectra of all three cobalt samples featured a peak at 73.5 eV. In addition, a broad peak between 70 and 55 eV was observed, with a maximum at roughly 61 and 60 eV. The XPS spectra of Raney-Co also included a shoulder at approximately 57 eV.

The peak at 73.5–73.9 eV is readily attributed to alumina (Al $2p^{3/2}$ emission line): α-Al_2O_3 (73.8 eV [39]), γ-Al_2O_3 (73.5 eV [36]), or $Al(OH)_3$ (73.6 eV [39]). (Note that this was the only state of aluminum in the cobalt samples.) In contrast, a contribution of metallic aluminum (72.3 eV [36]) was observed in the XPS spectrum of Raney-Ni at 72.3 eV. In this respect, it has been reported that Raney-Ni contains surface aluminum [22]. In the Co $3p^{3/2}$ region, both oxidized and metallic cobalt was found (61.3–61.7 and 59.2–60.0 eV, respectively), although the peak positions could not be clearly separated. The contribution of metallic cobalt increased after LiOH modification; Ni–Cr-promoted Raney-Co had the least intense metal contribution among the cobalt samples. This is in line with observations from the Co $2p^{3/2}$ region of the XPS spectra. The peak leading to the shoulder at 57 eV for Raney-Co indicates the presence of iron on the surface (Fe 3p line, FeOOH 56.3 eV [40]). Because XPS is much more sensitive for iron than for lithium, the Li 1s contribution in the XPS spectrum of the LiOH-modified Raney-Co (e.g., Li_2O 55.6 eV [41]) is difficult to evaluate. In contrast, iron was not observed for Ni–Cr-promoted Raney-Co. The XPS spectrum of Raney-Ni in the Ni $3p^{3/2}$ region shows mainly metallic nickel at 66.0 (66.3 eV [42]).

The elemental surface composition was estimated based on the main contributions of the XPS spectra (Table 5). Note that XPS mostly probes the outer surface of the catalyst particles. In the discussion of XPS data that follows, we assume that the composition of the inner and outer surfaces were comparable for the different catalysts. Raney-Co had little aluminum on the surface (4.1%), although these amounts were higher for Ni–Cr-promoted Raney-Co and Raney-Ni (5.3 and 13.7%, respectively). The amount of elemental cobalt or nickel on the surface was in the reverse order: 19.0% for Raney-Co, 17.9% for Ni–Cr-promoted Raney-Co, and 11.4% for Ni–Cr-promoted Raney-Ni. The corresponding ratios of elemental cobalt or nickel to aluminum were 4.6, 3.4, and 0.8, respectively. LiOH doping of Raney-Co led to an increase in the elemental ratio of cobalt to aluminum (6.9). As explained in the footnote to Table 5, determining the elemental surface composition of LiOH-modified Raney-Co was difficult because the contribution of iron and lithium could not be distinguished. Thus, this discussion is restricted to the ratios of the elements oxygen, cobalt, and aluminum.

Table 5
Estimation of the elemental surface composition of Raney-Ni, Raney-Co, Ni–Cr-promoted Raney-Co, and LiOH-modified Raney-Co by analysis of the XPS data

Element	Orbital	Raney-Ni [%]	Raney-Co [%]	Ni–Cr-promoted Raney-Co [%]	LiOH-modified Raney-Co[a] [%]
O[b]	1s	74.9	71.1	76.8	68.1–46.6–35.5
Co	3p	0	19.0	17.9	21.2–14.5–11.1
Ni	3p	11.4	–	–	–
Al	2p	13.7	4.1	5.3	3.0–2.1–1.6
Fe	3p	0	5.7	0	7.7–2.6–0
Li	1s	0	0	0	0–34.1–51.9

[a] Difficulties to separate Fe 3p and Li 1s lines led to ambiguities in the estimation of the iron and lithium content in LiOH modified Raney-Co. The three values shown were calculated assuming (i) 100% Fe, (ii) equal contribution of Fe and Li, and (iii) 100% Li, respectively. For the discussion, the values from assumption (ii) were considered most likely.

[b] The values exceed the real oxygen concentration on the surface as some carbon oxide contamination was unavoidable, which could not be distinguished from the metal oxide signal.

3.5. Adsorption of butyronitrile and n-butylamine from the liquid phase

Adsorption isotherms were recorded to characterize the (competitive) sorption properties of the catalysts. Isotherms derived from breakthrough curves [43] are shown in Fig. 8 (see Table 6 for adsorption capacities). The amount of *n*-butylamine adsorbed on the parent Raney-Co catalyst at saturation was significantly higher than the amount of adsorbed butyronitrile (7.39×10^{-2} and 5.37×10^{-2} mmol $g_{cat.}^{-1}$, respectively). After LiOH modification, the amount of *n*-butylamine decreased to 4.25×10^{-2} mmol $g_{cat.}{}^{-1}$ at saturation. Similarly, the adsorption capacity for butyronitrile was reduced after LiOH doping (4.06×10^{-2} mmol $g_{cat.}{}^{-1}$). Note that the intrinsic amount of adsorbents increased considerably on LiOH doping. Further, the adsorption capacity for butyronitrile increased relative to the adsorption capacity for *n*-butylamine after LiOH modification of the Raney-Co catalyst (ratios of 0.72 and 0.96, respectively).

Table 6
Amount of *n*-butylamine and butyronitrile adsorbed on Raney-Co and adsorption constants derived from break-through curves

Catalyst	*n*-Butylamine amount adsorbed		Butyronitrile amount adsorbed	
	[mmol $g_{cat.}{}^{-1}$]	[mol $mol_{Co,surface}{}^{-1}$]	[mmol $g_{cat.}{}^{-1}$]	[mol $mol_{Co,surface}{}^{-1}$]
Raney-Co	7.39×10^{-2}	0.185	5.37×10^{-2}	0.134
LiOH-modified Raney-Co	4.25×10^{-2}	0.236	4.06×10^{-2}	0.226

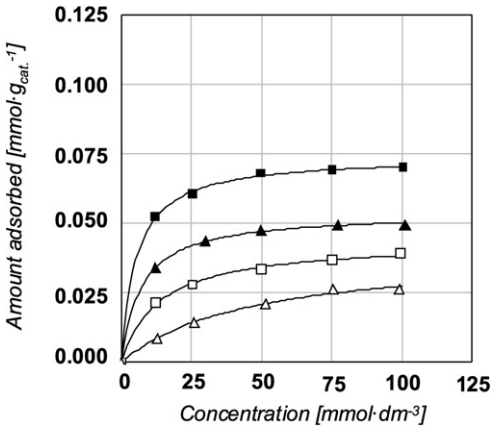

Fig. 8. Adsorption isotherms for adsorption of *n*-butylamine (■, □) and butyronitrile (▲, △) on parent (filled symbols) and LiOH-doped Raney-Co (open symbols) at 293 K. Solid lines represent a fit of the data according to the Langmuir equation.

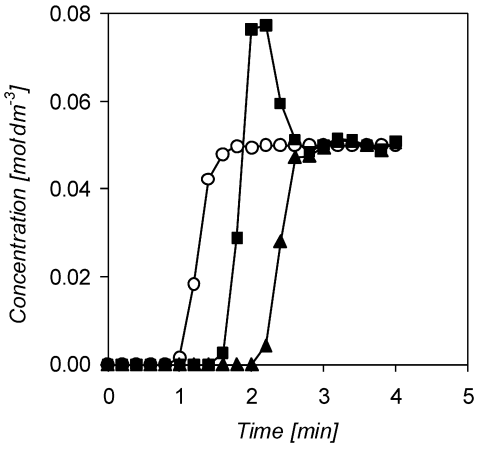

Fig. 9. Breakthrough curve for the co-adsorption of butyronitrile (■) and *n*-butylamine (▲) on Raney-Co at 293 K. Octane (○) was used as internal reference for determining the residence time distribution in the adsorption column.

To confirm the relative adsorption strength of *n*-butylamine and butyronitrile, competitive adsorption measurements were conducted on parent and LiOH-modified Raney-Co (Fig. 9). After the breakthrough of a nonadsorbing reference, butyronitrile appeared first in the eluent. The concentration of butyronitrile quickly rose above the feed concentration, passed through a maximum, and reached steady state at the same time as the breakthrough of *n*-butylamine occurred. This indicates that both molecules adsorb on the same sites and that the steady-state surface coverage was higher for *n*-butylamine than for butyronitrile (0.053 and 0.003 mmol $g_{cat.}{}^{-1}$, respectively, at 0.05 mol dm^{-3} adsorbent concentration). After LiOH doping, the molar ratio of *n*-butylamine and butyronitrile adsorbed on the catalyst surface at steady state decreased significantly (from 17.7 to 3.4).

4. Discussion

4.1. Reaction mechanism and role of surface intermediates in byproduct formation

A general mechanism for the formation of byproducts during the hydrogenation of nitriles was first proposed by von Braun in 1923 [44]. According to this model, the hydrogenation of butyronitrile proceeds via butan-1-imine, which is further hydrogenated to the primary butylamine. Secondary and tertiary amines are formed by desorption of the imine-intermediate from the catalyst surface, which subsequently reacts in solution with *n*-butylamine or di-*n*-butylamine (Fig. 10). Elimination of ammonia yields *N*-butylidene-butylamine and *N*-but-1-enyl-dibutylamine as condensation products. Subsequent hydrogenation provides di-*n*-butylamine and tri-*n*-butylamine.

The postulated intermediate butan-1-imine was not found in the reaction mixture. However, the transient concentration of butan-1-imine will be very low if it is consumed much faster than it is formed. Closer inspection of the time–concentration diagram showed that the formal condensation product of butan-1-imine and *n*-butylamine, *N*-butylidene-butylamine, was a primary kinetic reaction product. This strongly suggests that butan-1-imine or other intermediates taking part in the first step of byproduct formation did not desorb into the liquid phase, as was also suggested by a previous study [45]. The model also predicts the formation of *N*-but-1-enyl-dibutylamine as the precursor for tri-*n*-butylamine. Huang and Sachtler [45] detected *N*-but-1-enyl-dibutylamine in the liquid-phase over PdNi/NaY, although in a very low concentration. However in this study, we observed no *N*-but-1-enyl-dibutylamine and, only in case of the Raney-Ni catalyst, traces of tri-*n*-butylamine.

Thus, the side product *N*-butylidene-butylamine most likely results from a bimolecular condensation reaction occurring on the catalyst surface. Similar to the metal-catalyzed disproportionation of amines [46], the reaction is thought to proceed by condensation of unsaturated intermediates [47]. It was suggested that for nickel, carbenes and nitrenes can be formed as surface intermediates (see Fig. 11), with nitrenes being the preferred species [48]. In the initial step of the condensation reaction, a nitrogen nucleophile attacks an unsaturated carbon atom, such as the carbon atom of a carbene or a π-coordinated nitrile. This step of the condensation process is probably acid-catalyzed [30,49]. Note that nitrenes are much less susceptible to nucleophilic attack, because the carbon atom is fully saturated [47]. These surface processes depend on the catalyst

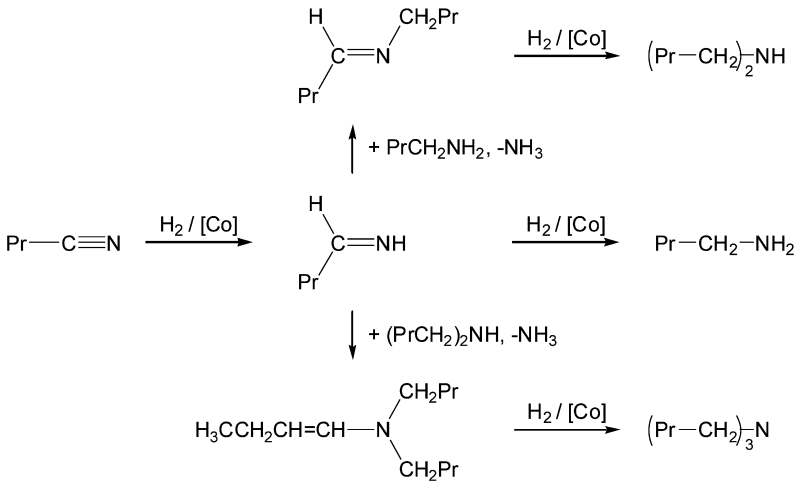

Fig. 10. Von Braun mechanism explaining the formation of higher amines during the reduction of butyronitrile with molecular hydrogen.

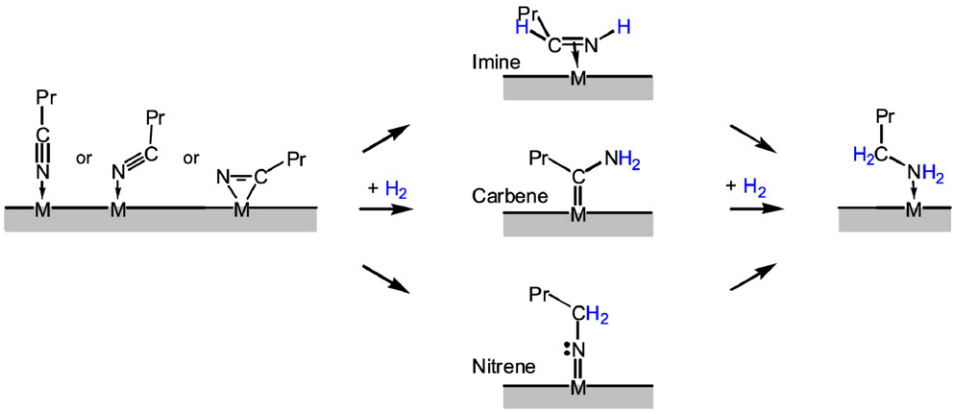

Fig. 11. Surface reactions suggested for the hydrogenation of butyronitrile.

properties and thus need to be addressed in the discussion on differences in selectivity and activity observed for the four types of catalysts.

4.2. Accessible metal atoms, oxidation state of the surface atoms, and the presence of Lewis acid sites

N_2-physisorption and H_2-chemisorption provided similar trends in the four catalysts even though different sites were probed. The catalyst with the highest BET surface area (Ni–Cr-promoted Raney-Co) had the highest concentration of accessible metal atoms. Thus, with an increasing BET area, it was possible to reach a better dispersion of the catalytically active metal. However, XPS measurements showed that the metal surface was in large part (>70%) covered with multioxide deposits, which do not contribute to the number of accessible metal atoms. XPS data also demonstrated that the aluminum content on the surface followed the trend in the bulk.

Accordingly, nickel in Raney-Ni was covered by aluminum oxide to a much larger extent than cobalt in Ni–Cr-promoted Raney-Co and Raney-Co. For Raney-Ni, Raney-Co, and Ni–Cr-promoted Raney-Co, the surface aluminum content was higher than in the bulk, indicating enrichment of aluminum in the surface near region. In TPD of NH_3, a high-temperature peak at 704–713 K was observed for those three catalysts and associated with ammonia desorbing from Al^{3+} Lewis acid sites. It appears likely that the Al^{3+} Lewis acid sites are associated with aluminum oxide on the catalyst surface. The nature of this surface oxide is strongly influenced by modification of the catalyst with LiOH. The TPD of NH_3 indicates that LiOH modification led to blocking of the sites associated with strong Lewis acidity, and we speculate that $LiAl_2(OH)_7$ was formed.

Consequently, one possible reason for the enhanced selectivity after LiOH addition is the reduced concentration of Lewis acid sites, which are known to catalyze condensation reactions [30]. A large part of the oxide deposit was removed during LiOH modification, and the fraction of the clean metal surface increased, as indicated by XPS.

The elemental ratio of the catalytically active metal to alumina and metal oxide was much lower for Raney-Ni, which is a possible explanation for the low selectivity to primary amine. Modification of Raney-Co with LiOH led to a decrease in the number of accessible metal atoms. However, the elemental ratio of cobalt to alumina was increased, indicating that on the one hand, surface alumina was removed or blocked, whereas on the other hand, LiOH covered part of the previously accessible metal atoms. By taking into account that the pore volume remained constant while the BET area was reduced, it can be

concluded that the decrease in accessible metal atoms was due to blocking of micropores, which contribute little to the pore volume.

4.3. The role of hydrogen in the reaction mechanism

Assuming a simple Langmuir–Hinshelwood model and surface reaction of the first hydrogen atom with adsorbed nitrile as the rate-determining step, the rate can be expressed as $r = k\theta_H\theta_{\text{butyronitrile}}$. Little dependence of the reaction rate on nitrile concentration was observed for all catalysts up to about 80% conversion. This observation is in line with previous liquid-phase hydrogenation reactions, for which zero order in nitrile was reported [50,51]. This suggests that the sites were fully saturated with nitrile during most of the reaction. Under the assumption of a Langmuir–Hinshelwood model, this observation leads to two possible scenarios concerning the co-adsorption of hydrogen and *n*-butyronitrile. The simpler of these scenarios is that hydrogen and nitrile adsorb on different sites. Alternatively, hydrogen and nitrile might compete for the same sites, but nitrile is adsorbed much more strongly. For nickel, more than one metal atom is required for adsorption of one acetonitrile molecule (up to 4) [48]. The resulting space between two nitrile molecules might be available for hydrogen adsorption. Thus, the scenario of different adsorption sites appears more likely. The hydrogen atoms can adsorb in different binding modes (e.g., on top, bridging, in hollow sites) that have different reactivities. In this respect, it has been reported that for nickel surfaces, on top bound hydrogen is less strongly adsorbed than hydrogen on bridge and hollow sites and thus is notably more reactive [48,52].

4.4. Effect of the sorption mode on activity and selectivity

The activation of the C≡N group depends on the sorption mode (see Fig. 11) and the strength of the interaction between nitrile and the metal surface. The nitrile group is able to bind with the C≡N bond normal to the surface plane (the preferred mode on cobalt, weak activation) or tilted, with the nitrile σ- and π-orbitals interacting with the surface (the preferred mode on nickel, strong activation) [53,54]. A metallacycle can also be formed, but this is not considered in the discussion here.

To gain insight into the influence of Li^+ on the adsorption of butyronitrile and *n*-butylamine, the adsorption of both molecules from the liquid phase was explored (Figs. 8 and 9). The findings were in line with the results from XPS and H_2-chemisorption measurements. Less butyronitrile and butylamine was adsorbed after LiOH doping (with respect to catalyst weight), reflecting an overall reduction in the number of accessible cobalt atoms. It is remarkable that in both cases, the coverage was <0.25 mol $\text{mol}_{\text{Co,surface}}{}^{-1}$. In this respect, theoretical results suggest that acetonitrile adsorbs on nickel preferentially parallel to the surface in a 4-fold or even 5-fold mode [48,55]. Taking into account that, due to the presence of oxidic species and alumina on the surface, not all elemental cobalt atoms are in groups of adequate size, the low coverage can be explained. The "steric" constraint around the adsorption sites might be reduced after LiOH doping, accounting for the higher adsorption capacity. The ratio of adsorbed butyronitrile (*n*-butylamine) to cobalt atoms on the surface decreased from 1:7.5 (1:5.4) to 1:4.4 (1:4.2) after LiOH modification.

The higher surface concentration of reactants is a possible reason for the higher activity observed after LiOH doping. The co-adsorption experiment on Raney-Co (Fig. 9) also showed that butyronitrile was partially displaced by *n*-butylamine, suggesting that both competed for the same sites. The rate remained constant up to relatively high conversion (80%). Thus, we tend to attribute the higher activity after LiOH doping to the lower amount of butylamine relative to butyronitrile adsorbing on the catalyst surface, leading to a higher surface concentration of butyronitrile for the LiOH-modified samples. With respect to selectivity, note that, due to the lower surface concentration of *n*-butylamine, the integral rate of condensation reactions, which involve amines, is reduced.

5. Conclusion

To gain insight into the critical properties affecting the selectivity and catalytic activity of Raney catalysts in the hydrogenation of nitriles, LiOH-modified Raney-Co and three commercial Raney catalysts (Raney-Ni, Raney-Co, and Ni–Cr-promoted Raney-Co) were tested and thoroughly characterized. Among the commercial catalysts, Ni–Cr-promoted Raney-Co showed the highest activity and selectivity to *n*-butylamine.

LiOH modification of Raney-Co led to enhanced intrinsic activity (second highest) and the highest selectivity of the catalysts tested. This beneficial effect of LiOH was linked to the modified nature of the catalyst surface. Most likely, islands of lithium aluminate and lithium hydroxide were formed on the catalyst surface, leading to a higher ratio of metallic cobalt to oxidic cobalt and alumina and resulting in (i) a reduced number of Al^{3+} Lewis acid sites, which are claimed to catalyze side reactions; (ii) a higher sorption capacity per metal atom for butyronitrile and butylamine; and (iii) a higher ratio of adsorbed butyronitrile relative to butylamine.

Therefore, the activity is increased due to an increased surface concentration of butyronitrile and reduced product inhibition by butylamine. In terms of selectivity, a lower adsorption constant of butylamine compared with that of butyronitrile is beneficial, because adsorbed butylamine is necessary for byproduct formation.

Acknowledgments

The authors thank Air Products & Chemicals Inc. for their generous financial support, and Jeno Bodis for many stimulating discussions.

References

[1] M.G. Turcotte, T.A. Johnson, in: J.I. Kroschwitz (Ed.), Kirk-Othmer Encyclopedia of Chemical Technology, vol. 2, fourth ed., Wiley, New York, 1992, pp. 369–386.

[2] M. Serra, P. Salagre, Y. Cesteros, F. Medina, J.E. Sueiras, J. Catal. 209 (2002) 202.
[3] S. Alini, A. Bottino, G. Capannelli, R. Carbone, A. Comite, G. Vitulli, J. Mol. Catal. A Chem. 206 (2003) 363.
[4] A.G.M. Barrett, in: B.M. Trost (Ed.), Comprehensive Organic Synthesis, vol. 8, Reduction, Pergamon, Oxford, 1991, pp. 251–257.
[5] J. Barrault, Y. Pouilloux, Catal. Today 37 (1997) 137.
[6] P. Baumeister, M. Studer, F. Roessler, in: G. Ertl, H. Knözinger, J. Weitkamp (Eds.), Handbook of Heterogeneous Catalysis, vol. 5, Wiley–VCH, Weinheim, 1997, pp. 2186–2195.
[7] F. Medina, P. Salagre, J.E. Sueiras, J. Mol. Catal. 81 (1993) 363.
[8] P.N. Rylander, Catalytic Hydrogenation over Platinum Metals, Academic Press, New York/London, 1967, pp. 203–226.
[9] P. Schärringer, T.E. Müller, W. Kaltner, J.A. Lercher, Ind. Eng. Chem. Res. 44 (2005) 9770.
[10] M.S. Wainwright, in: G. Ertl, H. Knözinger, J. Weitkamp (Eds.), Preparation of Solid Catalysts, Wiley–VCH, Weinheim, 1999, pp. 28–43.
[11] G. Cordier, P. Fouilloux, N. Laurain, J.F. Spindler, US Patent No. 5,777,166, 1998, to Rhone-Poulene Chimie.
[12] T. A. Johnson, US Patent No. 5,869,653, 1999, to Air Products and Chemicals, Inc.
[13] A.F. Elsasser, US Patent No. 5,874,625, 1999, to Henkel Corporation.
[14] W. Huber, J. Am. Chem. Soc. 66 (1944) 876.
[15] P. Tinapp, Chem. Ber. Rec. 102 (1969) 2770.
[16] C. Mathieu, E. Dietrich, H. Delmas, J. Jenck, Chem. Eng. Sci. 47 (1992) 2289.
[17] W. Reeve, J. Christian, J. Am. Chem. Soc. 78 (1956) 860.
[18] A.J. Chadwell Jr., H.A. Smith, J. Phys. Chem. 60 (1956) 1339.
[19] J.P. Orchard, A.D. Tomsett, M.S. Wainwright, D.J. Young, J. Catal. 84 (1983) 189.
[20] S. Nishimura, M. Kawashuma, S. Inoue, S. Takeoka, M. Shimizu, Y. Takagai, Appl. Catal. 76 (1991) 19.
[21] F. Hochard-Poncet, P. Delichere, B. Moraweck, J. Jobic, A. Renouprez, J. Chem. Soc. Faraday Trans. 91 (1995) 2891.
[22] S.N. Thomas-Pryor, T.A. Manz, Z. Liu, T.A. Koch, S.K. Sengupta, W.N. Delgass, Catalysis of Organic Reactions, in: F. Herkes (Ed.), Chemical Industries Series, vol. 75, Dekker, New York, 1998, p. 195.
[23] G. Moretti, in: G. Ertl, H. Knözinger, J. Weitkamp (Eds.), Handbook of Heterogeneous Catalysis, vol. 2, VCH–Wiley, Weinheim, 1997, pp. 632–641.
[24] J.R. Anderson, Structure of Metallic Catalysts, Academic Press, London, 1975, p. 228.
[25] A.B. Fasman, in: F. Herkes (Ed.), Catalysis of Organic Reactions, in: Chemical Industries Series, vol. 75, Dekker, New York, 1998, pp. 151–168.
[26] J.L. Falconer, J.A. Schwarz, Catal. Rev. Sci. Eng. 25 (1983) 141.
[27] G.A. Martin, P. Fouilloux, J. Catal. 38 (1975) 231.
[28] M. Nayak, T.R.N. Kutty, V. Jayaraman, G. Periaswamy, J. Mater. Chem. 7 (1997) 2131.
[29] J.P. Thiel, C.K. Chiang, K.R. Poeppelmeier, Chem. Mater. 5 (1993) 297.
[30] M.J.F.M. Verhaak, A.J. van Dillen, J.W. Geus, Catal. Lett. 26 (1994) 37.
[31] M.J.F.M. Verhaak, A.J. van Dillen, J.W. Geus, Appl. Catal. A 105 (1993) 251.
[32] Gmelins Handbuch der Anorganischen Chemie, System-Nr. 58: Kobalt, Ergänzungsband, Teil A, Verlag Chemie, Weinheim, 1961, p. 511.
[33] A. Baiker, M. Maciejewski, J. Chem. Soc. Faraday Trans. 1 80 (1984) 2331.
[34] A. Borgna, R. Frety, M. Primet, M. Guenin, Appl. Catal. 76 (1991) 233, and references therein.
[35] Y. Okamoto, J. Cryst. Growth 191 (1998) 405.
[36] C.D. Wagner, W.M. Riggs, L.E. Davis, J.F. Moulder, in: G.E. Muilenberg (Ed.), Handbook of X-Ray Photoelectron Spectroscopy, first ed., Perkin–Elmer Corporation (Physical Electronics Division), Eden Prairie, MN, 1979.
[37] T. Yoshino, T. Abe, I. Nakabayashi, J. Catal. 118 (1989) 436.
[38] D. Briggs, M.P. Seah (Eds.), Practical Surface Analysis, vol. 1, second ed., Wiley, New York, 1993.
[39] T.L. Barr, J. Vac. Sci. Technol. A 9 (1991) 1793.
[40] D. Brion, Appl. Surf. Sci. 5 (1980) 133.
[41] J.P. Contour, A. Salesse, M. Froment, M. Garreau, J. Thevenin, D. Warin, J. Microsc. Spectrosc. Electron. 4 (1979) 483.
[42] N.S. McIntyre, M.G. Cook, Anal. Chem. 47 (1975) 2208.
[43] A. Dabrowski, M. Jaroniec, Adv. Colloid Interface Sci. 31 (1990) 155.
[44] J. von Braun, G. Blessing, F. Zobel, Ber. 56B (1923) 1988.
[45] Y. Huang, W.M.H. Sachtler, Appl. Catal. A 182 (1999) 365.
[46] A. Ozaki, Isotopic Studies of Heterogeneous Catalysis, Kodansha Ltd./Academic Press, Tokyo/London, 1977, 140–141.
[47] B. Coq, D. Tichit, S. Ribet, J. Catal. 189 (2000) 117.
[48] B. Bigot, F. Delbecq, A. Millet, V.-H. Peuch, J. Catal. 159 (1996) 383.
[49] P. Sykes, A Guidebook to Mechanism in Organic Chemistry, sixth ed., Longman, London/Singapore, 1986.
[50] H. Li, Y. Wu, H. Luo, M. Wang, Y. Xu, J. Catal. 214 (2003) 15.
[51] B.W. Hoffer, P.H.J. Schoenmakers, P.R.M. Mooijman, G.M. Hamminga, R.J. Berger, A.D. van Langeveld, J.A. Moulijn, Chem. Eng. Sci. 59 (2004) 259.
[52] F. Hochard, H. Jobic, J. Massardier, A. Renouprez, J. Mol. Catal. A 95 (1995) 165.
[53] F.J.G. Alonso, M.G. Sanz, V. Riera, Organometallics 11 (1992) 801.
[54] A. Chojecki, H. Jobic, A. Jentys, T.E. Müller, J.A. Lercher, Catal. Lett. 97 (3–4) (2004) 155.
[55] B. Bigot, F. Delbecq, V.-H. Peuch, Langmuir 11 (1995) 3828.